Debonding of FRP and thin films from an elastic half-plane using a coupled FE-BIE model

Enrico Tezzon, Antonio Tralli, Nerio Tullini*

Department of Engineering, University of Ferrara, Via Saragat 1, Ferrara, Italy

e-mail: enrico.tezzon@unife.it; antoniomichele.tralli@unife.it; nerio.tullini@unife.it

*corresponding author

ABSTRACT

A Finite Element-Boundary Integral Equation (FE-BIE) coupling method is proposed to investigate a flexible bar weakly attached to an elastic orthotropic half-plane. Firstly, the analysis focused on the case of a bar subjected to horizontal forces and thermal loads considering interfacial displacements linearly proportional to the tangential traction. Secondly, the debonding behaviour of a composite reinforcement glued to a substrate has been modelled. Using an incremental nonlinear analysis, a bilinear elastic-softening interfacial traction-slip law has been implemented simulating the delamination of pure Mode II. Finally, the influence of the anchorage length on the ultimate bearing capacity of the adhesive joint has been investigated.

Keywords: Mixed variational principle, Green function, Weak interface, Debonding, FRP–strengthening concrete.

1 INTRODUCTION

In the last few decades, strengthening of existing concrete and masonry structures [1], and rehabilitation of steel structures [2] have emerged as a cutting edge issue in structural engineering. Particularly, the use of Fibre Reinforced Polymer (FRP) strips has become more and more common than ever before, as it has proved to be a rapid and efficient technical solution. Moreover, thin film-based devices and coated systems have been widely employed, remarkably in fields of aerospace and electronic engineering. There are plenty of studies focused on the issue of strengthening Reinforced Concrete (RC) members with externally bonded FRP sheets [3]. For these applications, a simple reference model may be a straight elastic stiffener of prescribed length bonded to an elastic substrate in plane state that can debond in pure mode II only. Moreover, bending stiffness of the stiffener may be disregarded because of negligible thickness. Consequently, the stiffener is not able to sustain transverse loads and no peeling stresses can arise at the interface.

In 1932, Melan studied the problem of a point force applied to an infinite stiffener bonded to an infinite linear elastic sheet [4]. Several authors have reconsidered and extended Melan's problem, especially for stiffened plate in aircraft structures and FRP strengthened RC structures. Early studies concerning stiffeners welded to an elastic substrate have adopted a series approximation method to solve singular integral equations including a proper Green function, see [5] and references cited therein. Perfect adherence hypothesis was relaxed in [6], where the adhesive interface was substituted by a set of independent linear elastic springs. This classical assumption [7] is frequently referred to as weak or imperfect interface and for a soft thin adhesive connecting two adherents was justified making use of asymptotic expansion methods of the corresponding three-dimensional elastic problem [8]. However, correction terms may be required at the adhesive ends [9]. For the case of an FRP plate glued to a rigid substrate, a closed-form analytical solution of shear-out test has been presented in [10], assuming an elastic-softening bilinear bond law at the adhesive interface and fracture behaviour in Mode II along the interface. In the same framework, the effect of the substrate elasticity has been considered in [11, 12], using a series approximation method.

Alternatively, a stress analysis combined with linear elastic fracture mechanics can be used to evaluate the critical delamination condition for RC beams strengthened with FRP strips [13].

Finite element procedures based on continuum damage models are required whenever the fracture behaviour involves the substrate [14, 15, 16]. Accurate results have been obtained in [17-20] using a regularized extended FE approach to interpret delamination tests in FRP strengthened concrete. Nonetheless, the FE approach undergoes important limitations when applied to film-substrate systems [21, 22] because a refined mesh has to be used to describe the thin layer of the film. Furthermore, to simulate the half-plane, FE meshes should be extended to a region significantly greater than the contact area; thus increasing the computational burden.

Boundary Element (BE) techniques can be used to evaluate the mechanical behaviour of coated systems involving thin layers, provided that the nearly-singular integrals arising in the BE formulations are correctly handled [23, 24]. Symmetric Galerkin boundary element techniques for cohesive interface problems are presented in [25, 26], where the nonlinear behaviour has been localized at the interface only. Moreover, reference [26] considered both substrate and reinforcement as linear elastic bodies and showed that a bar model is computationally more efficient than that of a thin layer.

For bars and beams resting on two-dimensional substrates, a Finite Element-Boundary Integral Equation (FE-BIE) coupling method is well suited to provide very accurate solutions at a low computational cost. To date, several problems have been analysed with the FE-BIE coupling method, such as thin films bonded to an isotropic elastic substrate subjected to thermal or axial loads [27] and Euler-Bernoulli and Timoshenko beams in frictionless [29, 30] or adhesive contact [31, 32] with an elastic half-plane, including buckling problems [33, 34].

In particular, the FE-BIE coupling method makes use of a mixed variational formulation including the Green function of the substrate, and assumes as independent fields both the nodal displacements and the contact tractions. It is worth noting that only the structure in contact with the substrate boundary has to be discretized. In addition, the mechanical response of the half-plane is

represented through a weakly singular integral equation, whose solution is given analytically, avoiding singular and hyper-singular integrals typically involved in the classical BE formulation. For the mixed problem at hand, useful mathematical references are [35, 36], where well-posedness of the variational problem and the corresponding Galerkin solution are set in the proper functional framework.

In the present paper, the FE-BIE coupling method is used introducing a slip between a flexible bar and an elastic orthotropic half-plane. To the authors' knowledge, the present proposal represents a new contribution.

First, the slip is assumed linearly proportional to the interface reactions. The cases of a bar subjected to a point force or a uniform thermal variation are investigated.

In the second part of this paper, incremental nonlinear analysis of the proposed model is adopted to investigate the delamination of an FRP strengthened RC substrate. The analysis of the interfacial reaction turns out to be important to predict the detachment phenomenon. The governing parameters of constitutive laws for adhesive interfaces must generally be estimated from experiments. However, the experimental determination of the mechanical properties of an adhesive is a complex task. These properties can be obtained by shear-out tests adopting different layouts, such as single slipping test with fixed back side or double pull-out shear schemes [37, 38]. Simple formulations for debonding analysis are generally based on *a priori* analytical expressions describing the interface bond-slip law calibrated from experimental results. In these formulations, a fracture process in pure Mode II is considered, disregarding the effects due to interface normal tractions (peeling) and out-of-plane displacements (uplift). The interface peeling stress and uplift develop due to eccentricity between applied force and interface and can be experimentally observed through advanced optical systems [39]. Although these components affect the ultimate bearing capacity of the adhesive joint, their influence on the distribution of interface slip throughout the contact region is negligible [40].

In the present model, an incremental analysis with displacement control has been used assuming a bilinear bond-slip law, and the results have been compared with those of experimental tests and analytical formulations found in the literature.

2 VARIATIONAL FORMULATION

An elastic bar with length L and cross section A attached to an elastic half-plane is considered, as shown in Fig. 1. Reference is made to a Cartesian coordinate system (O, x, z) centred at the midsection of the bar, with the vertical axis z directed toward the half-plane and the x-axis placed along the interface. Both the bar and the semi-infinite substrate are made of homogeneous and isotropic solids. Elastic constants E_b and ν_b respectively denote the Young modulus and the Poisson coefficient of the bar, whereas E_s and ν_s characterise the substrate. Generalised plane stress or plane strain regimes are considered. For plane strain, the width b of the half-plane will be assumed unitary. The thickness of the coating is assumed thin, so making possible to neglect its bending stiffness. In the absence of peeling stresses, only tangential tractions $r_x(x)$ occur along the contact region. The bar is subjected to a generically distributed horizontal load $p_x(x)$ or thermal variation $\Delta T(x)$.

Unlike the perfect adhesion case proposed in [27], the relaxed adhesion is representative of the mechanical characteristics of the adhesive connecting the bar with the substrate. This assumption involves the loss of continuity between bar displacement $u_{x,b}$ and half-plane displacement $u_{x,s}$.

2.1 Total potential energy for the bar

The strain energy of a bar can be written as follows [28]:

$$U_{\text{bar}} = \frac{1}{2}\int_L E_0 A(x)\,[u'_{x,b}(x) - \alpha_0 \Delta T]^2 \,\mathrm{d}x, \tag{1}$$

where prime denotes differentiation with respect to x, and the Young modulus E_0 and the coefficient of thermal expansion α_0 of the bar are $E_0 = E_b$, $\alpha_0 = \alpha_b$ for a generalized plane stress, and $E_0 =$

$E_b/(1-\nu_b^2)$, $\alpha_0 = (1+\nu_b)\alpha_b$ for a plane strain state. Noteworthy, the axial force in the bar is $N(x) = E_0A(x)[u'_{x,b}(x)-\alpha_0\Delta T]$. The potential energy Π_{bar} can be written as the strain energy U_{bar} minus the work related to the external loads:

$$\Pi_{\text{bar}} = U_{\text{bar}} - b\int_L [p_x(x) - r_x(x)]\, u_{x,b}(x)\,\mathrm{d}\,x. \tag{2}$$

2.2 Total potential energy for the substrate

The solution to the elastic problem for a homogeneous isotropic half-plane loaded by a point force tangential to its boundary is referred to as the Cerruti solution [41]. For a point force $P_x(\hat{x})$ applied to the half-plane boundary at the coordinates $\hat{x}$ (Fig. 2), the closed form expression for the surface displacement $u_{x,s}(x) = g(x,\hat{x})\,P_x(\hat{x})$, where the Green function $g(x,\hat{x})$ is:

$$g(x,\hat{x}) = -\frac{2}{\pi E}\ln\frac{|x-\hat{x}|}{d}. \tag{3}$$

In Eq. (3), $E = E_s$ or $E = E_s/(1-\nu_s^2)$ in the plane stress or plane strain, respectively, and d is an arbitrary length associated with a rigid displacement. The horizontal displacement $u_{x,s}(x)$ due to the interfacial tractions $r_x(x)$ acting along the boundary between the half-plane and the bar can be found as

$$u_{x,s}(x) = \int_L g(x,\hat{x})\, r_x(\hat{x}) d\hat{x}\,. \tag{4}$$

Making use of the theorem of work and energy for exterior domains [42], it can be shown that the total potential energy Π_{soil} for the half-plane equals one half the work of external loads [27, 29]:

$$\Pi_{\text{soil}} = -\frac{b}{2}\int_L r_x(x)\, u_{x,s}(x)\,\mathrm{d}\,x\,. \tag{5}$$

By introducing Eq. (4) into Eq. (5), one obtains

$$\Pi_{\text{soil}} = -\frac{b}{2}\int_L r_x(x)\,\mathrm{d}\,x \int_L g(x,\hat{x})\, r_x(\hat{x})\,\mathrm{d}\,\hat{x}. \tag{6}$$

2.3 Total potential energy for the adhesive

A displacement jump occurs when a stiffener is glued to a support by means of an adhesive. In the following, the transmission traction r_x is assumed proportional to the slip $\Delta u_x = u_{x,b} - u_{x,s}$ between the bar and the half-plane displacements

$$r_x = k_x \, \Delta u_x \,, \tag{7}$$

where parameter k_x summarizes the mechanical characteristics of the interface [8]. Making use of Eq. (7), the total potential energy for the adhesive can be written as

$$\Pi_{\text{spring}} = \frac{b}{2} \int_L r_x(x) \, \Delta u_x(x) \, \mathrm{d}\, x - b \int_L r_x(x) \, \Delta u_x(x) \, \mathrm{d}\, x = -\frac{b}{2} \int_L \frac{r_x^2(x)}{k_x} \, \mathrm{d}\, x \,. \tag{8}$$

2.4 Total potential energy for the bar-adhesive-substrate system

Making use of Eqs. (2), (6) and (8), the total potential energy of the whole system turns out to be

$$\Pi(u_{x,b}, r_x) = \Pi_{\text{bar}} + \Pi_{\text{soil}} + \Pi_{\text{spring}} \,, \tag{9}$$

which is a mixed variational formulation represented by bar displacement $u_{x,b}$ and interfacial tangential tractions r_x along the contact region. Consequently, making use of Eq. (7), the half-plane displacement $u_{x,s} = u_{x,b} - r_x/k_x$.

For a bar attached to an orthotropic substrate having a plane of elastic symmetry coincident with the vertical plane xz, reference [32] showed that the orthotropic substrate behaves like an isotropic half-plane assuming an equivalent Young modulus $E = 2 \, c_1/(c_2 \, R_{11})$, where parameters c_1, c_2, R_{11} are reported in Appendix. Obviously, the stress field within the orthotropic substrate differs from that of the isotropic case.

3 FINITE ELEMENT MODEL

Both the bar and the substrate boundary are subdivided into FEs sharing the same mesh. The generic ith FE has a length $l_i = |x_{i+1} - x_{i,}|$ where x_i and x_{i+1} are the initial and end coordinates. Assuming a dimensionless local coordinate $\xi = x/l_i$, the nodal displacements $\mathbf{u}_{xi}$ of the bar characterize completely the axial displacement field in the generic ith FE by means of the vector $\mathbf{N}(\xi)$ containing the shape functions:

$$u_{x,b}(\xi) = [\mathbf{N}(\xi)]^{\mathrm{T}}\, \mathbf{u}_{x,i}\,, \tag{10}$$

In the following, either linear (N_1 = 1–ξ, N_2 = ξ) or quadratic Lagrange polynomials (N_1 = 1–3ξ+2ξ^2, N_2 = 4ξ(1–ξ), N_3 = ξ(2ξ–1)) are adopted.

Piecewise constant functions are used to interpolate the tangential tractions

$$r_x(\xi) = [\boldsymbol{\rho}(\xi)]^{\mathrm{T}}\, \mathbf{r}_{x,i}\,, \tag{11}$$

where $\mathbf{r}_{x,i}$ represents the vector of nodal tangential tractions and $\boldsymbol{\rho}(\xi)$ is assumed to be unitary along the generic FE.

Substituting Eqs. (10) and (11) into the variational principle (9) and assembling over all the elements, the potential energy takes the expression

$$\Pi\left(\mathbf{u}_x, \mathbf{r}_x\right) = \frac{1}{2}\mathbf{u}_x^{\mathrm{T}}\mathbf{K}_a\,\mathbf{u}_x - \mathbf{u}_x^{\mathrm{T}}\mathbf{f}_x + \mathbf{u}_x^{\mathrm{T}}\mathbf{H}_{xx}\,\mathbf{r}_x - \frac{1}{2}\mathbf{r}_x^{\mathrm{T}}\mathbf{G}_{xx}\,\mathbf{r}_x - \frac{1}{2}\mathbf{r}_x^{\mathrm{T}}\mathbf{G}_{kx}\,\mathbf{r}_x\ , \tag{12}$$

where $\mathbf{K}_a$ is the bar stiffness matrix and $\mathbf{f}_x$ the external load vector, whose elements take the usual form

$$k_{a,ij} = \frac{1}{l_i}\int_0^1 E_0 A_b(\xi) N_i'(\xi)\, N_j'(\xi)\,\mathrm{d}\xi\,, \tag{13}$$

$$f_{x,i} = \int_0^1 \left(N_i(\xi)\, p_x(\xi) b l_i + N_i'(\xi)\, E_0 A(\xi)\,\alpha_0 \Delta T\right)\mathrm{d}\xi\,. \tag{14}$$

The components of matrices $\mathbf{H}_{xx}$, $\mathbf{G}_{xx}$ and $\mathbf{G}_{kx}$ are given by the following expressions

$$h_{xx,ij} = b l_i \int_0^1 N_i(\xi)\,\rho_j(\xi)\,\mathrm{d}\xi\,, \tag{15}$$

$$g_{xx,ij} = b \int_{x_i}^{x_{i+1}} \rho_i(x)\,\mathrm{d}x \int_{x_j}^{x_{j+1}} g(x,\hat{x})\,\rho_j(\hat{x})\,\mathrm{d}\hat{x}\,, \tag{16}$$

$$g_{kx,ii} = b \int_{x_i}^{x_{i+1}} \rho_i^2(x) \big/ k_x\,\mathrm{d}x\ . \tag{17}$$

Imposing the potential energy (12) to be stationary, the solution of the problem can be written in the following matrix form

$$\begin{bmatrix} \mathbf{K}_a & \mathbf{H}_{xx} \\ \mathbf{H}_{xx}^{\mathrm{T}} & -(\mathbf{G}_{xx}+\mathbf{G}_{kx}) \end{bmatrix} \begin{Bmatrix} \mathbf{u}_x \\ \mathbf{r}_x \end{Bmatrix} = \begin{Bmatrix} \mathbf{f}_x \\ \mathbf{0} \end{Bmatrix}. \tag{18}$$

The formal solution to the system of equations (18) provides the nodal displacements and tangential tractions

$$\mathbf{r}_x = (\mathbf{G}_{xx}+\mathbf{G}_{kx})^{-1}\,\mathbf{H}_{xx}{}^{\mathrm{T}}\,\mathbf{u}_x\,, \tag{19}$$

$$(\mathbf{K}_a + \mathbf{K}_{\mathrm{soil}})\,\mathbf{u}_x = \mathbf{f}_x\,, \tag{20}$$

where $\mathbf{K}_{\mathrm{soil}}$ is the stiffness matrix for the substrate with weak interface, defined as:

$$\mathbf{K}_{\mathrm{soil}} = \mathbf{H}_{xx}\,(\mathbf{G}_{xx}+\mathbf{G}_{kx})^{-1}\,\mathbf{H}_{xx}{}^{\mathrm{T}}. \tag{21}$$

3.1 Prismatic bar subjected to uniform load and thermal variation

A prismatic bar element subjected to uniform load p_x and thermal variation ΔT is considered. In the case of linear Lagrange shape functions, bar stiffness matrix $\mathbf{K}_a$, vector of equivalent external load $\mathbf{f}_x$ and matrix $\mathbf{H}_{xx}$ for the ith FE become

$$\mathbf{K}_{a,i} = \frac{E_0 A}{l_i} \begin{bmatrix} 1 & -1 \\ -1 & 1 \end{bmatrix}, \tag{22a}$$

$$\mathbf{f}_{x,i} = p\,b\,l_i/2\,[1,1]^{\mathrm{T}} + E_0 A\,\alpha_0 \Delta T\,[-1,1]^{\mathrm{T}}\,, \tag{22b}$$

$$\mathbf{H}_{xx,i} = b\,l_i/2\,[1,1]^{\mathrm{T}}\,, \tag{22c}$$

whereas for quadratic Lagrange shape functions the same quantities take the expressions:

$$\mathbf{K}_{ai} = \frac{E_0 A}{3 l_i} \begin{bmatrix} 7 & -8 & 1 \\ -8 & 16 & -8 \\ 1 & -8 & 7 \end{bmatrix}, \tag{23a}$$

$$\mathbf{f}_{x,i} = p\, h\, l_i / 6\, [1, 4, 1]^{\mathrm{T}} + E_0 A\, \alpha_0 \Delta T\, [-1, 0, 1]^{\mathrm{T}}, \tag{23b}$$

$$\mathbf{H}_{xx,i} = h\, l_i / 6\, [1, 4, 1]^{\mathrm{T}}. \tag{23c}$$

Piecewise constant functions are used to interpolate r_x and the shape functions for the substrate tractions are assumed to be $\boldsymbol{\rho}(\xi) = 1$. Consequently, the components of matrix $\mathbf{G}_{xx}$ are given by

$$g_{xx,ii} = \frac{2b}{\pi E} l_i^2 \left(\frac{3}{2} - \ln l_i \right), \tag{24a}$$

$$\begin{aligned} g_{xx,ij} = \frac{2b}{\pi E} \Big[& \frac{3}{2} l_i l_j + G(x_{j+1} - x_{i+1}) - \\ & G(x_{j+1} - x_i) - G(x_j - x_{i+1}) + G(x_j - x_i) \Big] \quad \text{for } i \neq j, \end{aligned} \tag{24b}$$

where $G(x) = x^2/2\, \ln|x|$ and the contribution of the arbitrary length d has been omitted since rigid-body displacements can be imposed in post-processing analysis. For instance, the horizontal displacement at one bar end or at the bar midspan can be set to zero.

Finally, the interface adhesive represented by the independent springs is described by a diagonal matrix $\mathbf{G}_{kx}$ having the following components:

$$g_{kx,ii} = \frac{b l_i}{k_{x,i}}, \qquad g_{kx,ij} = 0 \quad \text{for } i \neq j, \tag{25a, b}$$

where $k_{x,i}$ is the stiffness value for the generic ith FE.

3.2 Solution and post-processing

The solution to the FE-BIE problem, i.e., the system of equations (18), gives nodal displacement of the bar $\mathbf{u}_x$ and substrate traction $\mathbf{r}_x$. Once the nodal values of the primary variables are known, the axial force $N = E_0 A\,(u'_{x,b} - \alpha_0 \Delta T)$ and the displacement of the substrate $u_{x,s} = u_{x,b} - r_x/k_x$.

In summary, the general flow of the analysis of a reinforcement bar resting on an elastic substrate requires that the following steps be taken:

- discretize bar and substrate boundary into FEs;
- calculate element matrices $\mathbf{K}_{ai}$, $\mathbf{H}_{xx,i}$ and vectors $\mathbf{f}_{x,i}$ for each element;
- assemble element matrices $\mathbf{K}_{ai}$ and vectors $\mathbf{f}_{x,i}$ into the global matrix $\mathbf{K}_a$ and vector $\mathbf{f}_x$;
- assemble element matrices $\mathbf{H}_{xx,i}$ into the global matrix $\mathbf{H}_{xx}$;
- calculate global matrices $\mathbf{G}_{xx}$ and $\mathbf{G}_{kx}$;
- solve the system of equations (18) for the primary variables $\mathbf{u}_x$ and $\mathbf{r}_x$;
- compute secondary variables $u_{x,s}$ and N.

4 NUMERICAL EXAMPLES

Similarly to [4, 27], the elastic response of the bar-substrate system is characterised by the parameter

$$\beta L = \frac{E\,b\,L}{E_0 A}. \tag{26}$$

Low values of βL characterise short bars stiffer than the substrate. In this case, the bar performs like an almost inextensible stiffener. Higher values of βL describe long bars bonded to stiff substrate. With regards to the weak interface, the following parameter is introduced:

$$\gamma L = \sqrt{\frac{k_x\,b\,L^2}{E_0 A}}\,. \tag{27}$$

Low values of γL characterise practically detached bars, whereas high values of γL correspond to almost perfectly attached bars.

In the present section, several loading cases of a bar weakly attached to the underlying half-plane are considered and discussed. In subsection 4.1, some common problems are studied assuming a linear elastic behaviour of the bond-slip law and comparisons with the perfect bond case are made. In subsection 4.2, the debonding of an FRP plate glued on a concrete substrate is analysed. Numerical results are compared with solutions and experimental results found in the literature.

4.1 Linear analysis

In this section, 512 equal FEs with quadratic interpolation are used to model the elastic bar. A bar subjected to a horizontal concentrated force or a uniform thermal variation is analysed.

4.1.1 Bar loaded by a horizontal point force P_x at one end

A flexible bar loaded by a horizontal point force P_x at one end is investigated assuming $\beta L = 10$, $\gamma L = 5$ and $\beta L = 10$, $\gamma L = \infty$ (perfect adhesion). Dimensionless values of displacements, axial forces and tangential tractions along the bar are reported in Fig. 3. With reference to the weak interface case, bar displacement $u_{x,b}$ and substrate displacement $u_{x,s}$ along the whole contact region are greater and smaller, respectively, than those corresponding to the perfect adhesion case (Fig. 3a). Bar axial force is greater than that obtained for perfect adhesion (Fig. 3b) and singularities observed in tangential traction at the ends of a perfectly bonded bar disappear in the presence of a weak interface (Fig. 3c). Fig. 4 shows the maximum tangential reaction $r_x(L/2)$ versus parameter γL. Remarkably, the value of $r_x(L/2)$ depends on γL almost linearly irrespective of the parameter βL. In particular, $r_x(L/2) = C\,\gamma\,P_x$, where $C = 1$ for $\beta L \geq 10$ and $\gamma L \geq 3$ and $C = 1.19$ for $\beta L = 1$ and $\gamma L \geq 4$.

4.1.2 Bar subjected to an uniform thermal variation

In this subsection, an elastic bar subjected to a uniform thermal variation is investigated. This case is similar to that of a bar symmetrically loaded by two equal opposite forces applied at the ends [5]. In particular, the axial displacement and the interfacial tangential traction of a bar subjected to a uniform thermal load ΔT coincide with those induced in the bar by two opposite axial forces of magnitude $P_x = E_0 A \alpha_0 \Delta T$ applied at the ends [5]. With regard to the discrete problem, assuming consecutive bar FEs leads the vector of equivalent external loads to be expressed as $\mathbf{f}_x = P_x$ [–1, 0, ..., 0, 1]^T, see Eq. (23b). The axial force of a bar subjected to two opposite forces P_x at the ends is equal to that of the same bar subjected to a thermal load ΔT increased by the quantity $E_0 A \alpha_0 \Delta T$.

Nondimensional values of u_x, N and r_x versus x/L are reported in Fig. 5 for $\beta L = 10$, $\gamma L = 5$ and $\beta L = 10$, $\gamma L = \infty$ (perfect adhesion). For the weak interface case, the absolute value of the bar displacement u_{xb} is greater than that of the perfect adhesion case (Fig. 5a). Differently from what is observed for the concentrated force at one end, the axial force N is smaller than that obtained for perfect adhesion (Fig. 5b). Tangential traction r_x varies almost linearly for $|x/L| \leq 0.2$ and rapidly grows toward the end sections. However, differently from the perfect adhesion case, no traction singularity occurs at the bar ends (Fig. 5c).

4.2 Incremental nonlinear analysis of a shear-out test

In the relevant literature, several shear-out tests are available, especially for FRP strengthened RC structures [37, 43]. The shear-out tests could be used to determine not only the ultimate bearing capacity but even the local bond-slip behaviour of the interface [44, 45]. The bilinear elastic-softening bond-slip relationship (Fig. 6) is the function that is most commonly adopted [46].

In this section, the debonding process in shear-out tests due to an horizontal force P_x applied at the right bar end is evaluated using an incremental analysis with displacement control. The debonding phenomenon occurs when the slip between the strip and the substrate attains a critical value that causes separation. Fracture behaviour in pure Mode II is assumed throughout the

interface that is characterised by a bilinear elastic-softening bond-slip relationship (Fig. 6). A linear ascending branch, described by the stiffness parameter $k_{x,E}$, reaches the elastic limit $r_{x,0}$ for $\Delta u_{x,e} = r_{x,0}/k_{x,E}$. Afterwards, a softening behaviour is activated, described by a linear descending branch with slope $k_{x,S}$. For slip values greater than $\Delta u_{x,u} = r_{x,0}/k_{x,E} + r_{x,0}/k_{x,S}$, no bond tractions can be transferred trough the interface.

The mechanical and geometrical properties proposed in [10, 46] are introduced based on the experimental results reported in [47]. In particular, the elastic modulus of the Carbon FRP (CFRP) plate is E_0 = 100 GPa, while b = 25.4 mm and A = 25 mm^2, resulting in a thickness of 0.98 mm. For the concrete substrate E = 30 GPa. Two specimens in plane stress state characterised by bond lengths 50 and 200 mm are analysed, with parameter βL equal to 15 and 61, respectively. A number of 64 equal FEs based on linear interpolation are used to model the shorter bar (50 mm), while 128 equal FEs are used for the second one (200 mm), which can describe the behaviour of a long bar. For convenience, in this case Cartesian coordinate system (O, x, z) is centred at the left bar end.

Because of the randomness of the mechanical properties of the concrete substrate, the calibration procedure outlined in [45] assumes that each specimen has different interface properties. For the short anchorage, traction limit $r_{x,0}$ = 6.9 MPa, stiffnesses $k_{x,E}$ = 135 N/mm^3 (γL = 1.9) and $k_{x,S}$ = 25 N/mm^3, and ultimate slip $\Delta u_{x,u}$ = 0.33 mm are assumed. For the long anchorage, $r_{x,0}$ = 5.0 MPa with $k_{x,E}$ = 5000 N/mm^3 (γL = 38), $k_{x,S}$ = 100 N/mm^3 and $\Delta u_{x,u}$ = 0.05 mm have been set.

Fig. 7 shows diagrams of applied force P_x versus end slip Δu_x (Figs. 7a, d), FRP axial strain $\varepsilon_{x,FRP}$ versus coordinate x along the bonding length (Figs. 7b, e), and interface tangential traction r_x, once again reported versus x (Figs. 7c, f), obtained from the proposed FE-BIE model for the short and long anchorages. The force-slip response computed for the short anchorage is compared in Fig. 7a with the closed-form solution proposed in [10] (dashed line with symbol ×), which assumes a rigid substrate. The substrate deformability, taken into account by the proposed FE-BIE model, reduces the end slip compared with a rigid support. The corresponding values of the FRP axial strain $\varepsilon_{x,FRP}$ throughout the bond length are shown in Fig. 7b for the elastic state (solid line) and the

softening state (dashed line). An exponential shape of the axial strain $\varepsilon_{x,\mathrm{FRP}}$ can be observed until the peak load $P_{x,\mathrm{D}}$ (i.e. point D in Fig. 7a) is reached. Subsequently, the trend of $\varepsilon_{x,\mathrm{FRP}}$ becomes linear, and decreases until a complete detachment is achieved. Poor agreement between numerical predictions and experimental results (solid diamonds in Fig. 7b) has been found. Indeed, the assumed bond law parameters take implicitly account of concrete strain field only in proximity of the interface and are more suited for the case of a rigid substrate [10]. Numerical models considering a two-dimensional substrate require an adjustment of the interface laws calibrated by using a one-dimensional model [26]. The main aim of the present example is to show how the proposed FE-BIE method is simple and effective. Nonetheless, a subsequent research may be devoted to find the most suitable interface law to be used in conjunction with the proposed FE-BIE method. The development of the interface tangential traction r_x can be clearly drawn from Fig. 7c. In early stages, an exponential shape of the traction is shown along the contact region. A transition stage starts when traction $r_x(L)$ equals $r_{x,0}$ (curve B in Fig. 7c), and continues until the traction limit $r_{x,0}$ is exceeded at any point of the contact region (curve D in Fig. 7c). Finally, the tractions progressively decrease up to the complete debonding.

The force-slip response computed for the long anchorage is shown in Fig. 7d, where a flat plateau is observed between stages E and G. Results similar to those reported in [10] have been obtained in terms of interface strength. However, different slip values have been obtained. This discrepancy may depend on different choices of stiffness parameters for the interface law, which are not clearly stated in [10]. Figs. 7e and 7f show the FRP axial strains $\varepsilon_{x,\mathrm{FRP}}$ and the substrate reaction, respectively, for both the elastic (solid line) and the softening (dashed line) states. Points A in Fig. 7d characterises the end of the elastic states, whereas points B, C, D are typical of an elastic-softening behaviours. Subsequently, the debonding states begin at points E and continue until points G. In the detachment zone, the FRP axial strain $\varepsilon_{x,\mathrm{FRP}}$ remains constant. The tangential tractions r_x are reported in Fig. 7f, where a progressive decrease in tractions occurs up to attainment of the complete debonding.

5 CONCLUSIONS

A coupled FE-BIE model has been proposed to investigate problems of axially loaded bars weakly attached to a homogeneous elastic substrate in plane stress and plane strain state. Bar FEs have been used to simulate thin structures, the behaviour of the semi-infinite substrate has been represented using a BIE, whereas a slip between bar and substrate has been introduced using a set of independent springs. The computational advantages of the proposed coupled FE-BIE formulation can be summarized as follows:

- the BIE has been evaluated analytically, so avoiding the singularities connected with its numerical evaluation;
- a symmetric system of equations is obtained, thus avoiding the computational cost due to the lack of symmetry of the BE coefficient matrix of the classical FE-BE formulations;
- only the contact surface underneath the bar has been discretized, dramatically reducing the computational cost. In fact, the resolving matrix has dimensions proportional to the number of the bar FEs, differently to the standard FE approaches in which the dimensions of the stiffness matrix describing accurately the bar-substrate system has to be several times the square of the number of the bar FEs.

Some numerical examples have been presented to show the effectiveness of the proposed formulation. From the linear analysis of a bar subjected to a horizontal point force P_x at one end, the following conclusions can be drawn:

- bar axial force is greater for weak interface than for perfect adhesion (Fig. 3b);
- singularities observed in interfacial tangential traction at bar ends for perfect adhesion disappear for weak interface (Fig. 3c);
- for any given value of bar-substrate parameter βL, the tangential traction at the loaded end increases linearly with interface parameter γL (Fig. 4).

From the linear analysis of a bar subjected to a uniform thermal variation ΔT, the following conclusions can be drawn:

- bar axial force is smaller for weak interface than for perfect adhesion (Fig. 5b);
- once again, no singularity is observed in tangential traction at bar ends if a weak interface is assumed (Fig. 5c).

From the incremental nonlinear analysis of a shear-out test on a CFRP-strengthened RC substrate, the following conclusions can be drawn:

- the proposed FE-BIE model can be easily applied to study both short and long anchorages (Fig. 7);
- the substrate deformability reduces the interface slip compared with the case of rigid support (Fig. 7b);
- with regard to axial strain of the CFRP plate, the discrepancy observed between present analysis and experimental results reported in [47] require an adjustment of the elastic stiffness to be used in the bond-slip law. This aspect is well known as the bond-slip law is particularly sensitive to the adopted numerical model. A subsequent research may be devoted to find a bond-slip model more suitable for use in the proposed FE-BIE method.

ACKNOWLEDGMENTS

The present investigation was developed in the framework of the Italian PRIN Fund No. 2015LYYXA8 and of the Research Program FAR 2018 of the University of Ferrara. Moreover, the analyses were developed within the activities of the (Italian) University Network of Seismic Engineering Laboratories–ReLUIS in the research program funded by the (Italian) National Civil Protection – Progetto Esecutivo 2014-2018 – Research Line “Reinforced Concrete Structures”.

APPENDIX

In plane stress state, the substrate coefficients c_1, c_2, R_{11} are given by

$$c_1 = \left(\frac{E_z}{E_x}\right)^{1/4}, \quad c_2 = \left(2 + \frac{\sqrt{E_x E_z}}{G_{xz}} - 2\,\nu_{xz}\left(\frac{E_z}{E_x}\right)^{1/2}\right)^{1/2}, \quad R_{11} = \frac{1}{E_x}, \tag{A.1a,b,c}$$

whereas in plane strain state the constants c_1, c_2, R_{11} become

$$c_1 = \left(\frac{E_z}{E_x}\frac{1-\nu_{xy}\nu_{yx}}{1-\nu_{zy}\nu_{yz}}\right)^{1/4}, \tag{A.2a}$$

$$c_2 = \left(2 + \sqrt{\frac{E_z}{(1-\nu_{xy}\nu_{yx})(1-\nu_{zy}\nu_{yz})}}\left(\frac{\sqrt{E_x}}{G_{xz}} - \frac{2(\nu_{xz}+\nu_{xy}\nu_{yz})}{\sqrt{E_x}}\right)\right)^{1/2}, \tag{A.2b}$$

$$R_{11} = \frac{1-\nu_{xy}\nu_{yx}}{E_x}. \tag{A.2c}$$

where E_i denotes the Young modulus along the directions $i = x, z$, G_{ij} and ν_{ij} are the shear modulus and Poisson ratio, respectively, associated with directions $i, j = x, y, z$. In particular, due to this special kind of material symmetry, $\nu_{ij}/E_i = \nu_{ji}/E_j$. For an isotropic substrate, the coefficients reduce to $c_1 = 1$, $c_2 = 2$.

REFERENCES

[1] Bakis C, Bank L, Brown V, Cosenza E, Davalos J, Lesko J, Machida A, Rizkalla S, Triantafillou T. Fiber-reinforced polymer composites for construction - State of the art review. J Compos Constr 2002;6(2):73–87.

[2] Zhao X L, Zhang L. State of the art review on FRP strengthened steel structures. Eng Struct 2007;29(8):1808–23.

[3] Teng JG, Chen JF, Smith ST, Lam L. FRP strengthened RC structures. Chichester: John Wiley & Sons; 2001.

[4] Grigolyuk EI, Tolkachev VM. Contact problems in the theory of plates and shells. Moscow: Mir Publishers; 1987.

[5] Lanzoni L. Analysis of stress singularities in thin coatings bonded to a semi-infinite elastic substrate. Int J Solids Struct 2011;48(13):1915–1926.

[6] Lenci S. Melan's problems with weak interface, J Appl Mech - Trans ASME 2000;67(1):22–28.

[7] Goland M, Reissner E. The stresses in cemented joints. J Appl Mech - Trans ASME 1944;11:A17–A27.

[8] Geymonat G, Krasucki F, Lenci S. Mathematical analysis of a bonded joint with soft thin adhesive, Math Mech Solids 1999;4(2):201–225.

[9] Rizzoni R, Dumont S, Lebon F, Sacco E. Higher order model for soft and hard elastic interfaces. Int J Solids Struct 2014;51(1):4137-4148.

[10] Caggiano A, Martinelli E, Faella C. A fully-analytical approach for modelling the response of FRP plates bonded to a brittle substrate. Int J Solids Struct 2012;49(17):2291–2300.

[11] Franco A, Royer-Carfagni G. Cohesive debonding of a stiffener from an elastic substrate. Compos Struct 2014; 111:401–414.

[12] Franco A, Royer-Carfagni G. Effective bond length of FRP stiffeners. Int J Non-Linear Mech 2014;60:46–57.

[13] Rabinovitch O. Fracture-mechanics failure criteria for RC beams strengthened with FRP strips – a simplified approach. Compos Struct 2004;64(3–4):479–492.

[14] Wu Z, Yin J. Fracturing behaviors of FRP-strengthened concrete structures. Eng Fract Mech 2003;70(10):1339–1355.

[15] Lu XZ, Ye LP, Teng JG, Jiang JJ. Meso-scale finite element model for FRP sheets/plates bonded to concrete. Eng Struct 2005;27(4):564–575.

[16] Benzarti K, Freddi F, Frémond F. A damage model to predict the durability of bonded assemblies. Part I: Debonding behaviour of FRP strengthened concrete structures. Constr Build Mater 2011;25(2):547–555.

[17] Benvenuti E, Vitarelli O, Tralli A. Delamination of FRP-reinforced concrete by means of an extended finite element formulation. Compos Part B Eng 2012;43(8):3258–3269.

[18] Benvenuti E, Ventura G, Ponara N, Tralli A. Variationally consistent eXtended FE model for 3D planar and curved imperfect interfaces. Comput Meth Appl Mech Eng 2013;267:434–457.

[19] Benvenuti E, Orlando N, Ferretti D, Tralli A. A new 3D experimentally consistent XFEM to simulate delamination in FRP-reinforced concrete. Compos Part B Eng 2016;91:346–360.

[20] Benvenuti E, Orlando N. Failure of FRP-strengthened SFRC beams through an effective mechanism-based regularized XFEM framework. Compos Struct 2017;172:345–358.

[21] Zhang Y-M, Gu Y, Chen J-T. Internal stress analysis for single and multilayered coating systems using the boundary element method. Eng Anal Bound Elem 2011;35(4):708–717.

[22] Zhang Y, Li X, Sladek V, Sladek J, Gao X. A new method for numerical evaluation of nearly singular integrals over high-order geometry elements in 3D BEM. J Comput Appl Math 2015; 277:57–72.

[23] Zhang Y-M, Qu W-Z, Chen J-T. BEM analysis of thin structures for thermoelastic problems. Eng Anal Bound Elem 2013; 37(2):441–452.

[24] Gu Y, Chen W, Zhang B. Stress analysis for two-dimensional thin structural problems using the meshless singular boundary method. Eng Anal Bound Elem 2015;59:1–7.

[25] Salvadori A. A symmetric boundary integral formulation for cohesive interface problems. Comput Mech 2003;32(4–6):381–391.

[26] Freddi F, Savoia M. Analysis of FRP–concrete debonding via boundary integral equations. Eng Fract Mech 2008;75(6):1666–1683.

[27] Tullini N, Tralli A, Lanzoni L. Interfacial shear stress analysis of bar and thin film bonded to 2D elastic substrate using a couple FE-BIE method. Finite Elem Anal Des 2012;55:42–45.

[28] Szabó B, Babuška I. Finite Element Analysis. New York: John Wiley & Sons; 1991.

[29] Tullini N, Tralli A. Static analysis of Timoshenko beam resting on elastic half-plane based on the coupling of locking-free finite elements and boundary integral. Comput Mech 2010;45(2–3):211–225.

[30] Baraldi D, Tullini N. Incremental analysis of elasto-plastic beams and frames resting on an elastic half-plane. J Eng Mech 2017; 134(9): Article number 04017101, 1-9.

[31] Tezzon E, Tullini N, Minghini M. Static analysis of shear flexible beams and frames in adhesive contact with an isotropic elastic half-plane using a coupled FE-BIE model. Eng Struct 2015;104:32–50.

[32] Tezzon E, Tullini N, Lanzoni L. A coupled FE-BIE model for the static analysis of Timoshenko beams bonded to an orthotropic elastic half-plane. Eng Anal Bound Elem 2016;71:112–128.

[33] Tullini N, Tralli A, Baraldi D. Stability of slender beams and frames resting on 2D elastic half-space. Arch Appl Mech 2013;83(3):467–482.

[34] Tullini N, Tralli A, Baraldi D. Buckling of Timoshenko beams in frictionless contact with an elastic half-plane. J Eng Mech 2013; 139(7): 824–831.

[35] Kikuchi N, Oden J. Contact problems in elasticity: A study of variational inequalities and finite element methods, SIAM, Philadelphia, 1988.

[36] Bielak J, Stephan E. A modified Galerkin procedure for bending of beams on elastic foundations, SIAM J Sci Stat Comput 1983; 4(2): 340–352.

[37] Ferracuti B, Mazzotti C, Savoia M. A new single-shear set-up for stable debonding of FRP–concrete joints. Constr Buil Mater 2008;23(4):1529–1537.

[38] Panigrahi S, Pradhan B. Onset and growth of adhesion failure and delamination induced damages in double lap joint of laminated FRP composites. Compos Struct 2008;85(4):326–336.

[39] Czaderski C, Soudki K, Motavalli M. Front and side view image correlation measurements on FRP to concrete pull-off bond tests. J Compos Constr 2010;14(4):451–464.

[40] Martinelli E, Czaderski C, Motavalli M. Modeling in-plane and out-of-plane displacement fields in pull-off tests on FRP strips. Eng Struct 2011;33(12):3715–3725.

[41] Johnson K L. Contact Mechanics, University Press, Cambridge, 1985.

[42] Gurtin ME, Sternberg E. Theorems in linear elastostatics for exterior domains, Arch Ration Mech Anal 1961;8(1):99–119.

[43] Yao J, Teng JG, Chen JF. Experimental study on FRP to concrete bonded joints. Compos Part B Eng 2005;36(2):99–113.

[44] Taljsten B. Defining anchor lengths of steel and CFRP plates bonded to concrete. Int J Adhes Adhes 1997;17(4):319–327.

[45] Lu XZ, Teng JG, Ye LP, Jiang JJ. Bond–slip models for FRP sheets/plates bonded to concrete, Eng Struct 2005; 27: 920–937.

[46] Faella C, Martinelli E, Nigro E. Direct versus indirect method for identifying FRP to concrete interface relationships. J Compos Constr 2009;13(3):226–233.

[47] Chajes MJ, Finch WW, Januska TF, Thomson TA. Bond and force transfer of composite material plates bonded to concrete. ACI Struct J 1996;93(2):208–217.

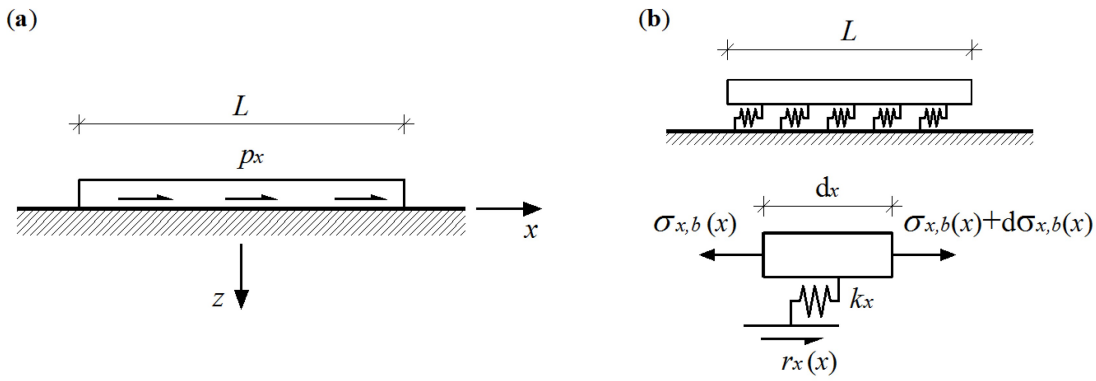

Fig. 1. Bar weakly attached to a semi-infinite substrate (**a**), and free-body diagram (**b**).

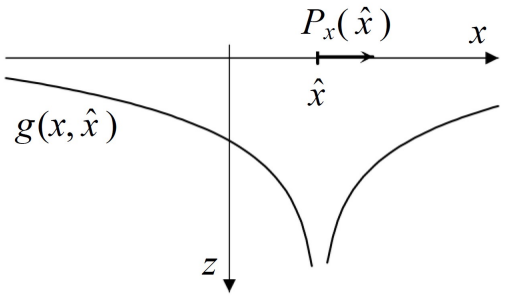

Fig 2. Green's function $g(x,\hat{x})$ related to a point force $P_x(\hat{x})$ applied to the half-plane boundary.

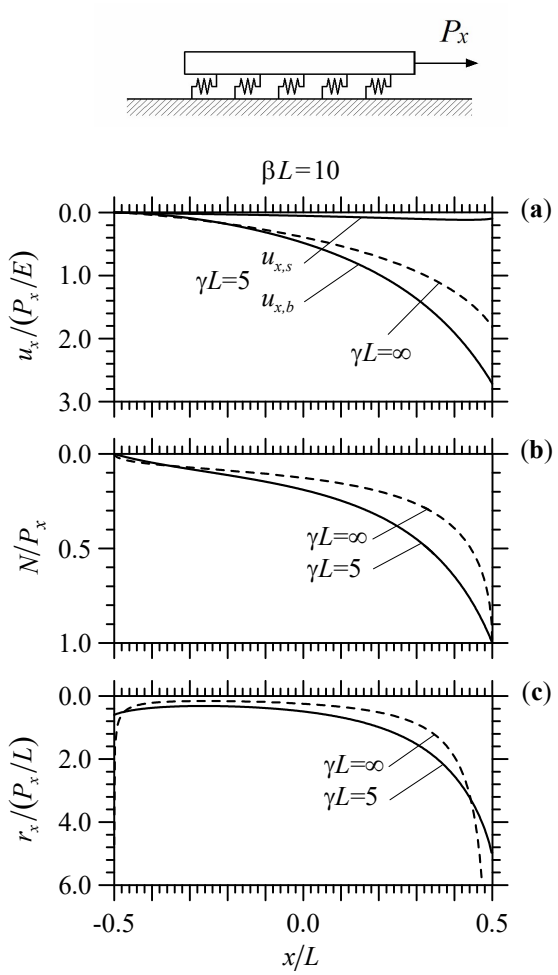

Fig. 3. Bar loaded by a point force P_x at one end. Nondimensional values of u_x (**a**), N (**b**) and r_x (**c**) versus x/L for $\beta L = 10$, $\gamma L = 5$ (solid line) and $\beta L = 10$, $\gamma L = \infty$ (dashed line - perfect adhesion).

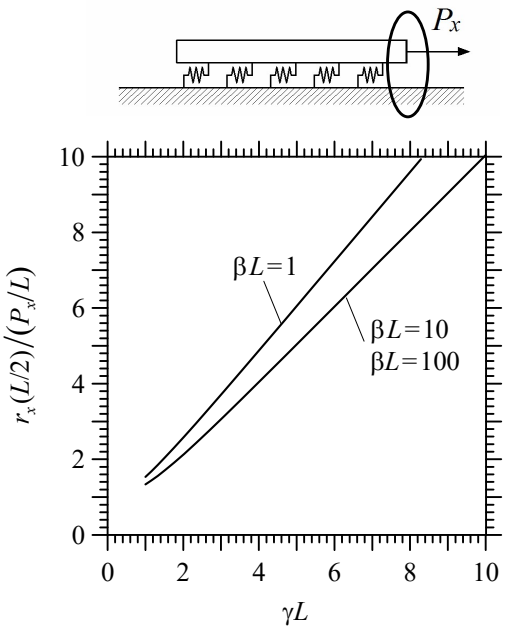

Fig. 4. Bar loaded by a point force P_x at one end. Nondimensional values of r_x at the loaded end ($x/L = 0.5$) versus γL.

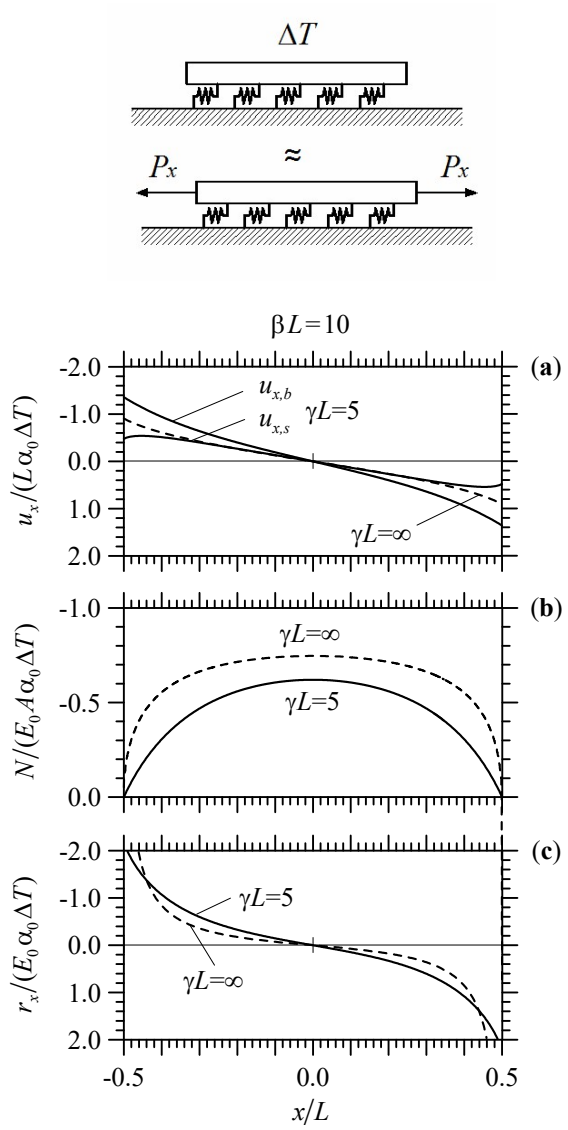

Fig. 5. Bar subjected to a uniform thermal variation ΔT. Nondimensional values of u_x (**a**), N (**b**) and r_x (**c**) versus x/L for $\beta L = 10$, $\gamma L = 5$ (solid line) and $\beta L = 10$, $\gamma L = \infty$ (dashed line - perfect adhesion).

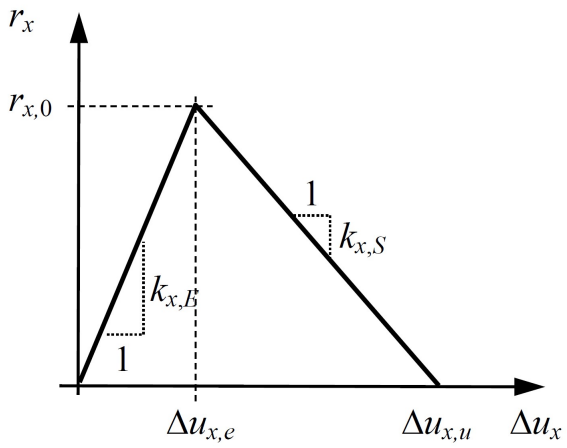

Fig. 6. Bilinear bond-slip law.

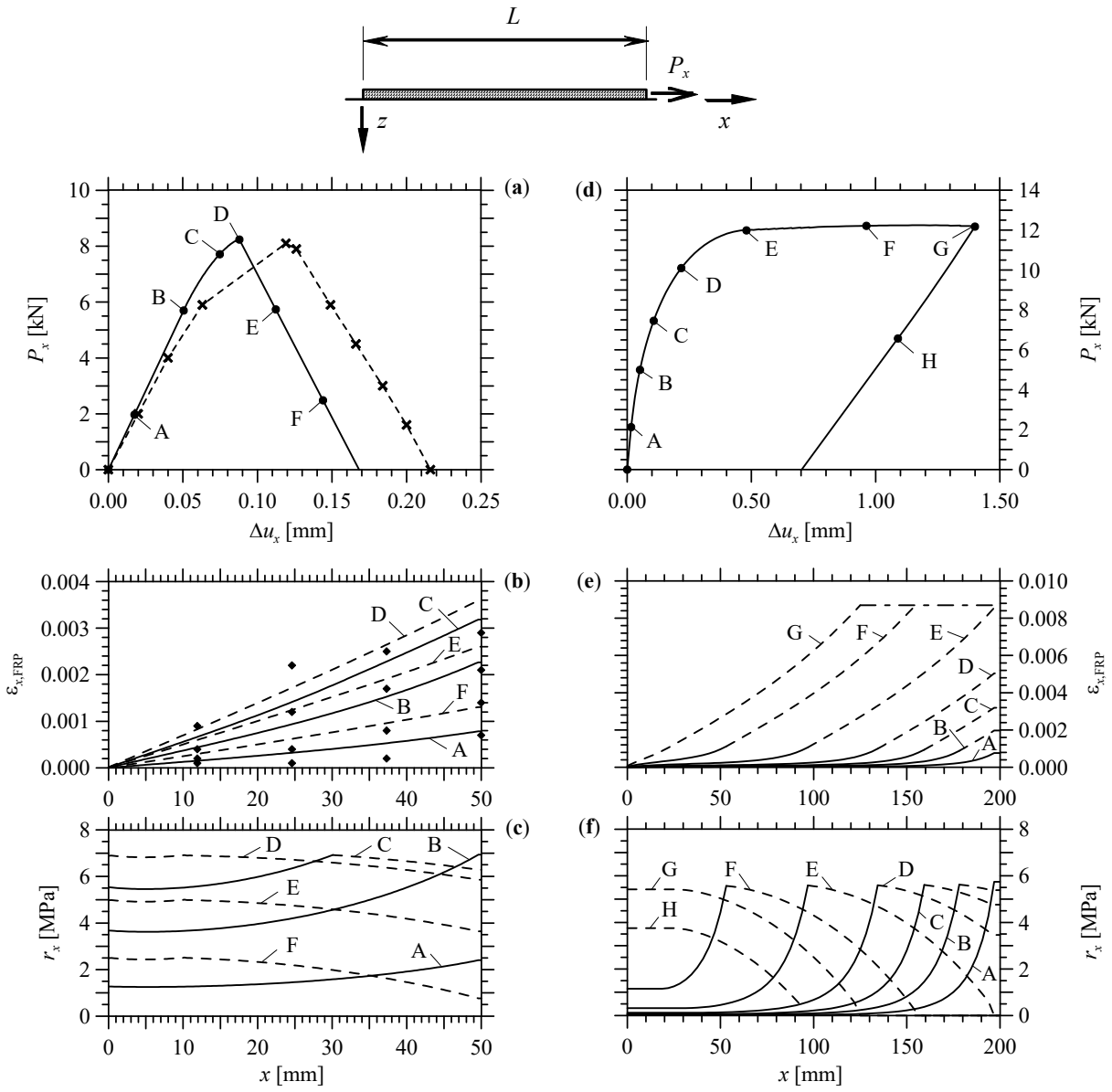

Fig. 7. Incremental nonlinear analysis of a shear-out test on short (**a**, **b**, **c**) (L = 50 mm) and long (**d**, **e**, **f**) anchorage. Applied force P_x vs. end slip Δu_x (**a**, **d**), FRP axial strain $\varepsilon_{x,\mathrm{FRP}}$ (**b**, **e**) and interface traction r_x (**c**, **f**) along the bonding length. Comparison with analytical results reported by Caggiano et al. (dashed line with symbol (×) in (**a**)) and experimental results reported by Chajes et al. (solid diamonds in (**b**)).